



Regular article

Wavelength selection of bidirectional laser transmission based on Monte Carlo method

Chuanxin Zhang^a, Xusheng Zhang^b, Yuan Yuan^{a,*}, Qing Ai^{a,*}, Heping Tan^a^a School of Energy Science and Engineering, Harbin Institute of Technology, 92, West Dazhi Street, Harbin 150001, PR China^b Changchun Institute of Optics, Fine Mechanics and Physics, Chinese Academy of Sciences, Changchun 130033, PR China

HIGHLIGHTS

- A model of transient radiative transfer of bidirectional path laser was developed.
- The radiative characteristics of five different spectral bands were calculated.
- The optimal bands were determined in different atmospheric conditions.

ARTICLE INFO

Article history:

Received 23 April 2017

Revised 11 May 2017

Accepted 11 May 2017

Available online 13 May 2017

Keywords:

Transient radiative transfer

Active laser detection

Imaging simulation

Atmospheric scattering

ABSTRACT

The laser detection technology in uncertain and dynamic environments is of utmost importance in many fields. A model of transient radiative transfer of bidirectional path laser based on Monte Carlo method is developed to investigate the optimum wavelength of active detector at complex atmospheric conditions. The radiative parameters of atmosphere are calculated by HITRAN database and Mie theory at several typical atmospheric conditions including the standard atmosphere, urban aerosol, and radiation fog. Transmission characteristics for five spectral bands at the above atmospheric conditions are calculated by this model. The optimal transmission ability occurred in bands 0.2–0.5, 1.4–1.6, and 0.75–1.25 μm on the condition of standard atmosphere, urban aerosol, and radiation fog, respectively. All results provide effective reference and basic support for choosing the optimal spectral band for active detection.

© 2017 Elsevier B.V. All rights reserved.

1. Introduction

The laser detection technology in uncertain and dynamic environments is of utmost importance for laser ranging, Lidar, and resources exploration [1,2]. Laser detection can be divided into active detection and passive detection according to whether the system needs illuminant or not [3,4]. The passive detection technology has been studied deeply because it can provide coverage of wide areas at a moderate running cost [5–9]. System itself does not carry illuminant, which detects by using the radiation of target and surrounding. Target signal is easily submerged by the background in inclement weather, such as dominated backward scattering, which cause a poor resolution. It leads to be difficult to clearly recognize and identify the remote target [10–12]. The active laser detection technology can overcome most of the drawbacks of passive one [13–15,3,16]. Combined with range gate technique, the signal noise ratio of target echoes would be effectively improved [17].

A lot of papers have been published on active laser detection and range-gated imaging. Zhang and Sun analyzed the effects of divergence angle, incident angle and detection distance on the active laser detection system [3]. Zhang et al. proposed a comb-based active laser ranging scheme for enhanced distance resolution and a common time standard for the entire system [18]. Chen et al. presented a method of active laser ranging over interplanetary distances with asynchronous two-way ranging which is validated in real time laboratory experiments and field tests [19]. Degnan developed the models for various sources of noise in an interplanetary transponder link which includes planetary albedo, solar or lunar illumination of the local atmosphere, and laser backscatter off the local atmosphere [20]. Busck and Heiselberg designed a fast and high-accuracy three-dimensional imaging laser radar based on range-gating segmentation [21]. Steinvall et al. systematically and experimentally investigated the laser radar model and range gating technique. They presented some advanced concepts for gated viewing including a spectral diversity illuminating technique for speckle reduction and bistatic configurations. And they discussed with respect to image quality and processing techniques during

* Corresponding authors.

E-mail addresses: yuanyuan83@hit.edu.cn (Y. Yuan), hitaiqing@hit.edu.cn (Q. Ai).

Nomenclature

a, b	control parameter of particle size distribution
c, c_0	speed of light in the medium and vacuum, respectively
\mathbf{e}_q	direction cosine
f	mirror-diffuse ratio
g	anisotropy factor
G	incident spectral radiation of time domain
I	radiative intensity
i, j, k	unit vector
L	transmission length
n	particle number per unit volume
P_{Laser}	incident power of Gaussian pulse peak
P_t	receive power of detection area
q_{ix}, q_{iy}, q_{iz}	scalar quantity in x, y, z direction, respectively
r_i, r_g	incident radius and mean radius of aerosol, respectively
R_θ, R_φ, R_L	random number
t_p	pulse time
W	width of rectangular

Greek symbols

$\kappa_{e\lambda}$	extinction coefficient
$\kappa_{a\lambda}$	absorption coefficient
$\kappa_{s\lambda}$	scattering coefficient
ω_λ	scattering albedo
Φ	scattering phase function
λ	wavelength
v	space variance variable
ρ	reflectivity
Γ	Gamma function
σ_s	scattering coefficient
σ	mean square deviation
θ'	zenith angle
θ_c	critical angle
θ_i	incident angle of incident ray
θ_t	refraction angle of incident ray

different range and atmospheric conditions [22–24]. Several numerical methods, such as Monte Carlo (MC) method [25–27], discrete ordinate method [28–30], and finite-volume method [31], have been applied to the transient radiative transfer in recent years. The MC simulation is extremely suitable for solving transient radiative transfer as the conversions between space and time are easy to achieve. The full-spectrum calibration is usually used to carry out by the above methods [32]. However, wavelength selection is essential to gain better prediction performance [33–35]. Few papers studied the wavelength selection in complex atmosphere using bidirectional laser transmission based on Monte Carlo method. It motivated us to study this future.

This paper investigated the transient radiative transfer of pulse laser in two-dimensional participating medium by the MC method. A model of bidirectional path transient radiative transfer of pulse laser was developed in Section 2. The echo signal characteristics of pulse laser in different weather conditions at spectrum ranges of 0.2–2.2 μm were analyzed in Section 3. The adaptability of different wavelength lasers was discussed and the optimum wavelength in different weather conditions was given.

2. Method and model

2.1. Transient radiative transfer equation

The ultrashort pulse laser is characterized by a high peak intensity which is far greater than that of the medium self-radiation [36]. Transient radiative transfer equation in an absorbing, scattering and non-emitting medium can be written as

$$\frac{1}{c} \frac{\partial I_\lambda(s, \mathbf{s}, t)}{\partial t} + \frac{\partial I_\lambda(s, \mathbf{s}, t)}{\partial s} = -\kappa_{e\lambda}(s) I_\lambda(s, \mathbf{s}, t) + \frac{\kappa_{s\lambda}(s)}{4\pi} \times \int_{4\pi} I_\lambda(s, \mathbf{s}_i, t) \Phi_\lambda(\mathbf{s}_i, \mathbf{s}) d\Omega_i \quad (1)$$

where

$$\kappa_{e\lambda}(s) = \kappa_{a\lambda}(s) + \kappa_{s\lambda}(s) \quad (2)$$

Here, c is the propagation speed of light in the medium, Φ is scattering phase function, $\kappa_{a\lambda}$, $\kappa_{s\lambda}$, and $\kappa_{e\lambda}$ are the absorption, scattering, and extinction coefficients, respectively, and $I_\lambda(s, \mathbf{s}, t)$ is the radiative intensity at position s along direction \mathbf{s} at time t .

Assumed the property parameters of medium, including $\kappa_{a\lambda}$, $\kappa_{s\lambda}$, and $\kappa_{e\lambda}$, do not vary with location s . Divide both sides of Eq. (1) by $\kappa_{e\lambda}$, and the transient radiative transfer equation of pulse laser can be obtained on the spectral optical thickness τ_λ , which can be represented as

$$\frac{dI_\lambda(\tau_\lambda, \mathbf{s}, t)}{d\tau_\lambda} = -I_\lambda(\tau_\lambda, \mathbf{s}, t) + \frac{\omega_\lambda}{4\pi} \int_{\Omega_i=4\pi} I_\lambda(\tau_\lambda, \mathbf{s}_i, t) \Phi_\lambda(\mathbf{s}_i, \mathbf{s}) d\Omega_i \quad (3)$$

where $\tau_\lambda = \int_0^s \kappa_{e\lambda}(x) dx$, ω_λ is scattering albedo. Just absorption occurs when $\omega_\lambda = 0$ and scattering occurs when $\omega_\lambda = 1$.

The vector of radiative heat flux density of time domain $\mathbf{q}_\lambda(s, t)$ is written as Eq. (4). Incident spectral radiation of time domain $G_\lambda(s, t)$ is given by Eq. (5).

$$\begin{aligned} \mathbf{q}_\lambda(s, t) &= \int_{4\pi} I_\lambda(s, \mathbf{s}, t) \cdot \mathbf{e}_q d\Omega = \mathbf{i} q_{\lambda x}(s, t) + \mathbf{j} q_{\lambda y}(s, t) + \mathbf{k} q_{\lambda z}(s, t) \\ &= \mathbf{i} \int_{4\pi} I_\lambda(s, \mathbf{s}, t) \cos \theta d\Omega + \mathbf{j} \int_{4\pi} I_\lambda(s, \mathbf{s}, t) \cos \beta d\Omega + \mathbf{k} \int_{4\pi} I_\lambda(s, \mathbf{s}, t) \cos \gamma d\Omega \end{aligned} \quad (4)$$

$$G_\lambda(s, t) = \int_{4\pi} I_\lambda(s, \mathbf{s}, t) d\Omega \quad (5)$$

where $q_{\lambda x}$, $q_{\lambda y}$, $q_{\lambda z}$ is the scalar quantity along the Cartesian coordinates x , y , and z directions, respectively, \mathbf{e}_q is direction cosine, \mathbf{i} , \mathbf{j} , \mathbf{k} is unit vector.

2.2. Transmission probability model

Radiative intensity is defined by Eq. (6) according to Bouguer's law when the pulse laser transferred to an absorbing, scattering and non-emitting medium. The propagation distance and optical thickness of each random transfer in the MC method by Eqs. (7) and (8), respectively. The transmission time can be obtained by Eq. (9).

$$I_{\lambda, L} = I_{\lambda, 0} \exp(-\beta_\lambda L) \quad (6)$$

$$L_i = -\ln R_L / \beta_\lambda \quad (7)$$

$$\tau_{\lambda i} = -\ln R_L \quad (8)$$

$$t_i = L_i / c = n_i L_i / c_0 = n_i \tau_{\lambda i} / c_0 \beta_\lambda \quad (9)$$

where c_0 is the propagation speed of light in vacuum, n_i is the refractivity of medium, R_i is the random number between 0 and 1, L_i is the propagation distance, and t_i is the transmission time. The relationship between initial and final positions can be shown as

$$\begin{cases} x_1 = x_0 + L_0 \sin \theta_0 \cos \varphi_0 \\ y_1 = y_0 + L_0 \sin \theta_0 \sin \varphi_0 \\ z_1 = z_0 + L_0 \cos \theta_0 \end{cases} \quad (10)$$

where (x_0, y_0, z_0) and (x_1, y_1, z_1) are the initial and final position, respectively, (θ_0, φ_0) is the direction of initial light, L_0 is the propagation distance.

The direction of light propagation after scattering is determined by the scattering phase function. Since scattering in air and water is characterized by the Henyey-Greenstein phase function Eq. (11), which gives a sharp forward scattering peak [37,38].

$$\Phi(\theta) = (1 - g^2)/(1 + g^2 - 2g \cos \theta)^{1.5} \quad (11)$$

where θ is the scattering angle, g is the asymmetry factor and a property parameter of the material which determine the shape of phase function, $-1 \leq g \leq 1$. It can be used to generate a primarily forward scattering function ($g < 0$) or a primarily backward scattering function ($g > 0$) or an isotropic function ($g = 0$).

The exact analytical solution can be expressed as

$$\cos \theta = \frac{1}{2g} \left[1 + g^2 - \left(\frac{1 - g^2}{1 - g + 2gR_L} \right)^2 \right] \quad (12)$$

where the random $\cos \theta$ can be achieved by generating a set of uniformly distributed value R_L following the distribution law. The probability model of scattering direction can be utilized for the MC simulation.

2.3. Comparison and verification

Consider transient radiative transfer in two-dimensional slab, as shown in Fig. 1. The two-dimensional case is as example used to validate the transient radiative transfer of laser in this section. The geometric dimensions are L in thickness in the z direction, W in width in the y direction, and infinite in the x direction [27]. The pulse laser is normally incident upon the participating medium from the origin of the Cartesian coordinates. Three detectors with detection radius r are equally located in the line between incident and exit plane. The basic values of parameters are $L = 10$ mm, $W = 10$ mm, $t_p = 10$ ps, $r_i = 1.0$ mm, $\beta_\lambda = 1.0$ mm⁻¹, $\omega_\lambda = 0.997$, $\Delta s = 2$ mm, $v = r_i$, $n_s = 1.33$, refractive index of surrounding environment n is 1.0. To compare the results of two conditions, the square input pulse and Gaussian input pulse are set in $[0, t_p]$ and $[-2t_p, 3t_p]$, respectively.

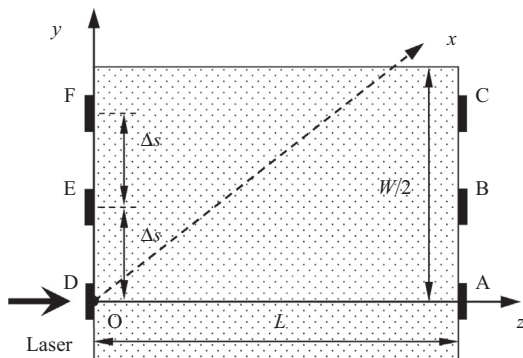


Fig. 1. Model of medium geometry and coordinates profiles of pulse laser incidence.

Combined the length and width of cross section, the location of each detector along with the Cartesian coordination can be calculated. Mirror reflection occurs at the interface. Fresnel reflection is taken into account at the input and output interfaces which are exposed to air. A linear anisotropic scattering phase function is adopted to analyze the variation of characteristics of transmission and reflection influenced by the scattering direction.

The reflectivity of two lateral sides ($y = W/2$ and $y = -W/2$) is 0, which means the incident lights are all absorbed by the lateral sides. For the incident face ($z = 0$) and transmission face ($z = L$), the reflectivity is 0 when the incident angle of interface is smaller than the critical angle, and the reflectivity is 1.0 when the incident angle of interface is greater than the critical angle. The bundles number is 1.0×10^7 . Signal characteristics of transmission and reflection of Gaussian pulse and square pulse is calculated. Comparisons of temporal transmissivity at three different detector locations subject to different temporal variations of Gaussian input pulse and square input pulse are shown in Figs. 2–5.

The results of reflectivity and transmissivity for each detector match well with Ref. [27], which further verify the correctness of the method and model. The volatility of transmissivity is stronger than that of reflectivity since the high scattering albedo of medium. The influence of time domain pulse shape on the signal distribution for each detection point is slight according to comparing the results of Gaussian pulse and square pulse.

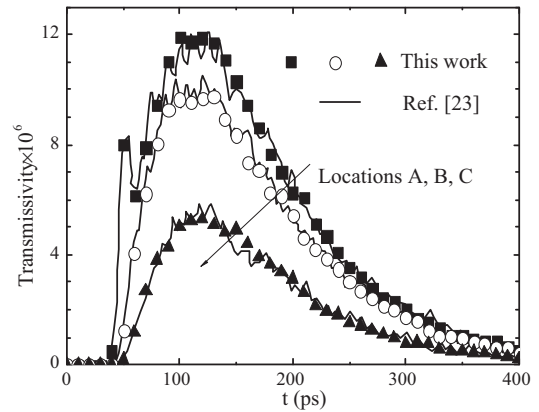


Fig. 2. Comparisons of temporal transmissivity at three different detector locations subject to different temporal variations of Gaussian input pulse.

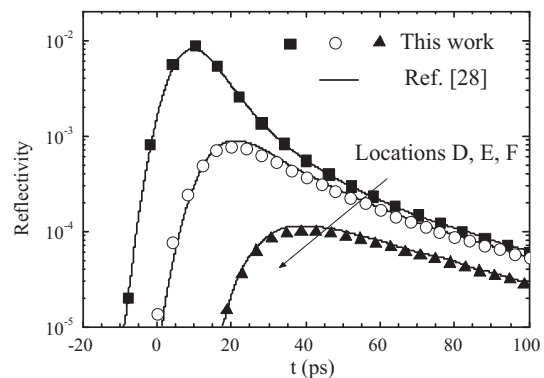


Fig. 3. Comparisons of temporal reflectivity at three different detector locations subject to different temporal variations of Gaussian input pulse.

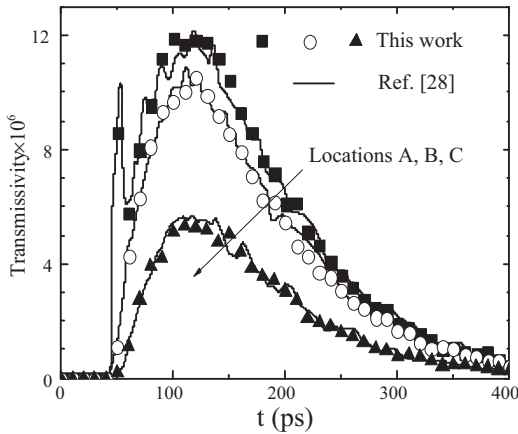


Fig. 4. Similar to Fig. 2 but for the square input pulse.

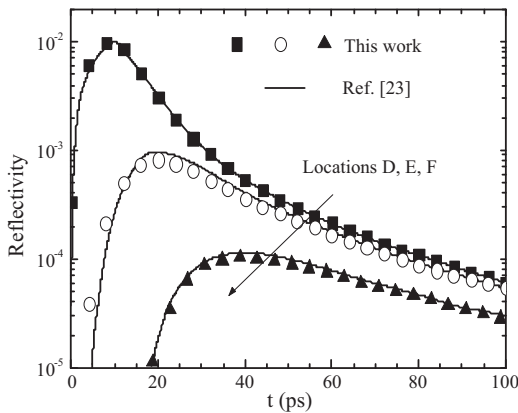


Fig. 5. Similar to Fig. 3 but for the square input pulse.

2.4. Atmosphere radiative transfer model

The model of atmospheric radiative transfer is established to study the optimum band of laser detection for different atmospheric conditions in this section. Simplified conditions are given as following:

- (1) The effect of earth curvature on the echo signal is omitted since that the altitude is much smaller than that of earth radius. Turbid atmosphere is regarded as a parallel plane layered structure.

- (2) The composition and property parameters of atmosphere vary with the altitude. The spectral extinction coefficient, scattering albedo, scattering phase function are constant in each layer.
- (3) Clouds, fogs and aerosols are composed of opaque uniform particles. The species and number density keep constant at the same altitude. The refractive index of turbid atmosphere including fogs and aerosols is as same as standard dry atmosphere.
- (4) Complex physical processes, such as atmosphere turbid effect, intense laser non-linear effect are omitted. The slight scattering effect of atmosphere media on pulse laser and autologous emitting effect is not taken into account.

The characteristics of spectral absorption and scattering of pulse laser are considered for the complex atmosphere medium. Scattering effect is generated by the particles which suspend in the standard atmosphere. The three-dimensional simplified transmission model which is infinity in horizon direction and layering in vertical direction is obtained. The standard structured grids are obtained by layering the space in the horizontal and vertical direction. The sketch of transient radiative transfer model in two layers media is shown as Fig. 6.

Pulse laser projected the upper surface of the second layer where radiative energy experienced absorption and scattering for many times. A part of energy returned back to the surface after reflection and scattering. Meanwhile, the rest energy transmitted the second layer and reached the first layer near the ground. The time which target signal and noise turned back the detector is different. Therefore, the energy of signal and noise can be differentiated according to controlling the switch time of strobing gate. Some energy of weak noise still existed in the target signal though the above technique is adopted. The transmission length of noise is as same as that of target signal in medium, which does not reach the target surface. Hence, it is necessary to analyze the signal noise ratio.

3. Results and discussion

The adaptability of laser transfer in different wavelengths and atmospheric conditions is investigated in this section. Absorption coefficients of standard atmosphere at 0.5–2 μm at 0–1 km is shown in Fig. 7. Absorption coefficients are small in some ranges, i.e., the corresponding transmission performance is better than others. The detection wavelengths are selected, which are shown in Table 1. The wavelength of band I and bands II–V are calculated by MODTRAN and HITRAN, respectively. Different atmospheric

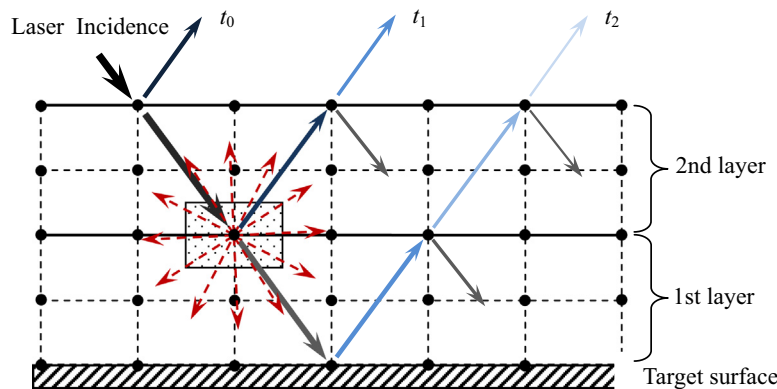


Fig. 6. Sketch of transient radiative transfer model in two layers media.

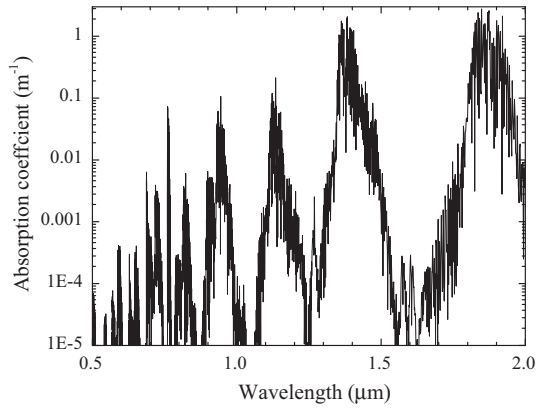


Fig. 7. Absorption coefficient of standard atmosphere.

conditions are shown in Table 2. The transmission performances of laser transfer in the conditions including different atmosphere conditions with various compositions are discussed.

3.1. Basic parameters and conditions

The effect of detection radius and reflection on characteristic of laser transfer is discussed in this section. Spectral absorption coefficient of standard atmosphere is calculated line-by-line at 0–1 km. Band mean absorption coefficient is obtained by the method of Planck mean absorption coefficient. The results are shown in Table 3. Spectral extinction coefficient increases with the increasing wavelength. The scattering effect is omitted and the scattering albedo is set to 0.0 since many small gas molecules exist in the standard atmosphere.

Basic values of parameters are $t_p = 10$ ns, $d_i = 30$ mm, $v = r_i$, pulse time duration is $0-5t_p$, detection point and incident point at same location, detection diameter is 100 mm, laser vertically incident to the medium, and the reflection coefficient of ground target ρ_λ^d is 1.0.

The concept of echo signal ratio (ESR) is adopted in order to elaborate this question. ESR is defined as the ratio of received power of detector and peak power of Gaussian pulse. It can be described as

$$ESR = \frac{P_t(\pi r_i^2, t)}{P_{\text{Laser}}(t = t_c)} \quad (13)$$

where P_t is the received power of detector at time t , P_{Laser} is the peak power of Gaussian pulse. The energy cannot be received by the detector if $ESR \leq 10^{-12}$.

The dependence of ESR on pulse time of band I when the detection radii are 0.5, 5.0 and 50 m are shown in Fig. 8. ESR increased obviously with the increasing detector radius. The peak values of the ESR shift to the right side with the increasing detection area. The perfect diffuse reflection and mirror reflection do not occur for the real target surface. Reflection characteristic of most material surface is between the mirror reflection and diffuse reflection. Mirror-diffuse reflection probability model which combined the mirror reflection and diffuse reflection of the MC method is proposed.

Table 1
Laser bands.

Bands	I	II	III	IV	V
Wavelength (μm)	0.2–0.5	0.5–0.75	0.75–1.25	1.25–1.4	1.4–1.6

Table 2
Different atmospheric conditions.

Altitude range	0–1 km
Atmospheric condition	Standard atmosphere Typical urban aerosol Urban aerosol and radiation fog

The light incidents the target surface with an angle θ ($0 < \theta < \pi/2$) in the local coordinate of reflection surface. Specular reflectivity is a function of pulse wavelength and incident angle, and the reflection direction is decided by Fresnel law. Diffuse reflectivity is related with wavelength. The mirror-diffuse ratio is used to describe the relationship of incident wavelength and roughness of target surface. Reflection characteristic of real target surface in local coordinate can be expressed as

$$\rho_\lambda^{s+d}(\theta) = f_0 \cdot \rho_\lambda^s(\theta) + (1 - f_0)\rho_\lambda^d \quad (14)$$

$$\begin{cases} \theta^{s+d} = \theta \\ \varphi^{s+d} = \varphi \end{cases} \quad (f \leq f_0) \quad (15)$$

$$\begin{cases} \theta^{s+d} = \arccos(\sqrt{1 - R_\theta}) \\ \varphi^{s+d} = 2\pi R_\varphi \end{cases} \quad (f > f_0) \quad (16)$$

where $\rho_\lambda^{s+d}(\theta)$ is the real spectral reflectivity of target surface, θ^{s+d} , φ^{s+d} are zenith angle and circumference angle of incident ray in local coordinate, respectively, R_θ , R_φ are both random number drawn from a uniform distributed between 0 and 1. f can control the reflection direction and reflectivity of real surface. $f = 0$, $f = 1$, and $0 < f < 1$ correspond to the conditions that the surface is diffuse reflection, mirror reflection and range between diffuse and mirror reflection, respectively.

Dependence of ESR on pulse time of five bands is shown as Fig. 9 when f is 1.0. ESR is greatly affected by the spectral extinction coefficient of dry atmosphere. On the other hand, initial respond time and the peak value of ESR is not affected by the spectral extinction coefficient. Normalization method was used to deal with the ESR results. ESR of different spectral extinction coefficient has the same time domain distribution, i.e., the extinction coefficient just affects ESR, and it does not affect the time spread of echo signal for dry atmosphere medium. Bands I, II and III have a better transmission at 0–1 km in clean and dry atmosphere, and the transmission decreases with the increasing extinction coefficient.

3.2. Urban aerosol

The aerosols with various types and size are suspended in the atmosphere even in clear weather condition, which has an extra absorption and scattering effect on pulse laser. The elaborated observation data of the aerosols in different time, place and altitude is lacking because of complex of types, concentration and size spectrum distribution at present. Radiative characteristic of aerosol is described by aerosol model in many papers [39–41]. Complex refractive index and size spectrum distribution are calculated by aerosol model, and the absorption and scattering index is determined by Mie scattering theory.

Considering the complicated characteristics of aerosol particles, some functions are used to determine the distribution of particles

Table 3
Spectral mean property parameters.

Bands	I	II	III	IV	V
Extinction coefficient (m^{-1})	1.68×10^{-5}	3.46×10^{-5}	9.78×10^{-5}	8.09×10^{-4}	1.78×10^{-3}

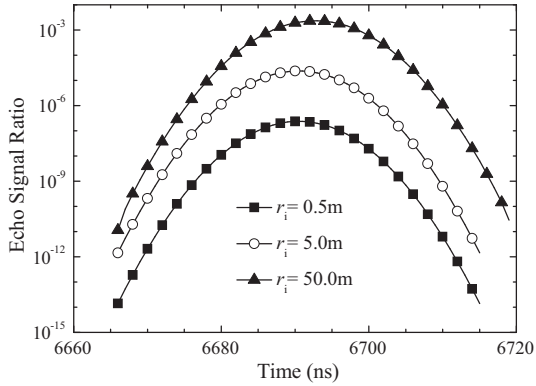


Fig. 8. Dependence of ESR on pulse time when the radii of detection are 0.5, 5.0 and 50 m.

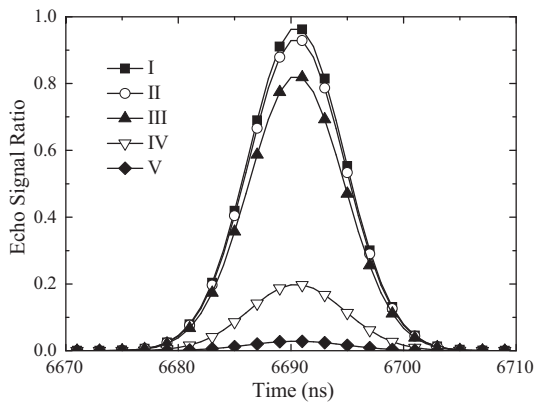


Fig. 9. Dependence of ESR on pulse time of five bands in standard atmosphere.

size [42,43]. The Log-normal distribution model is shown as following.

$$n(r) = \frac{1}{\sqrt{2\pi}\sigma} \frac{1}{r} \exp\left[-\frac{(\ln r - \ln r_g)^2}{2\sigma^2}\right] \quad (17)$$

where σ is mean square deviation, r_g is mean radius of aerosol. The number density is the biggest when $r = r_g$.

Turbid atmosphere of log-normal distribution is adopted. The spectral band mean parameters at 0–1 km and the results are shown in Table 4. It can be drawn that scattering albedo and the extinction coefficient of the aerosol is bigger than that of the dry atmosphere. Spectral extinction coefficient and scattering albedo are independent and different for bands since strongly spectral selection of aerosol particles.

Table 4
Mean property parameter of atmosphere with urban aerosol.

Bands	I	II	III	IV	V
Extinction coefficient (m^{-1})	9.29×10^{-2}	1.23×10^{-2}	4.42×10^{-3}	4.33×10^{-2}	4.27×10^{-3}
Scattering albedo	0.866	0.881	0.861	0.799	0.480

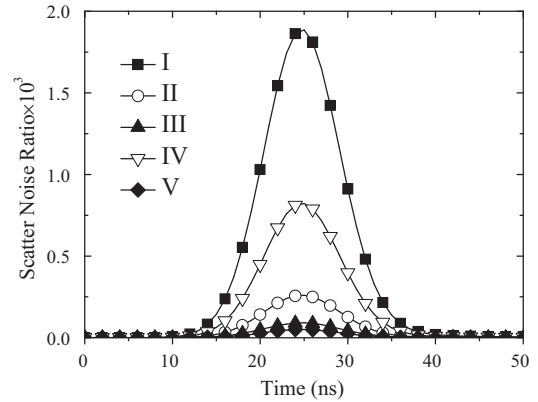


Fig. 10. Dependence of SNR on pulse time of five bands in aerosol atmosphere.

The received energy of the detector can be divided into signal energy which is reflected by the target surface and noise energy which undergoes several times scattering and is not reflected by the target surface. Target signal ratio (TSR) and scattering noise ratio (SNR) are proposed to describe scattering characteristic of atmosphere. The definition of TSR and SNR are shown as follows.

$$\text{TSR} = \frac{P_t^{\text{target}}(\pi r_i^2, t)}{P_{\text{Laser}}(t = t_c)} \quad (18)$$

$$\text{SNR} = \frac{P_t^{\text{noise}}(\pi r_i^2, t)}{P_{\text{Laser}}(t = t_c)} \quad (19)$$

where P_t^{target} and P_t^{noise} are the received target signal power and scattering noise, respectively. Obviously, ESR is the sum of TSR and SNR.

SNR and TSR of 5 bands are calculated at 0–1 km when $f = 1.0$. The results are shown in Figs. 10 and 11. Time which scattering noise signal arrives at the detector is earlier than that of the target. It can be seen from Fig. 10 that the time is at 0.0–50.0 ns, i.e., the detector receives SNR simultaneously when the pulse laser arrives at the medium. The value of SNR is biggest when the incident pulse peak is 25 ns. It can be seen from Fig. 11 that the TSR of bands I, II and IV are zero, and the detection target signal only exist in bands III and V. Spectral extinction coefficient is big when TSR is zero, which leads to loss most laser energy during the transfer process and only the rest tiny energy arriving at the target surface. The probability that the echo target lights arrive at the detector surface sharply decreases because of the small area of detector and large distance between target and detector. Band V has a stronger echo signal than that of band III since the spectral extinction coefficient of band V is bigger than that of band III.

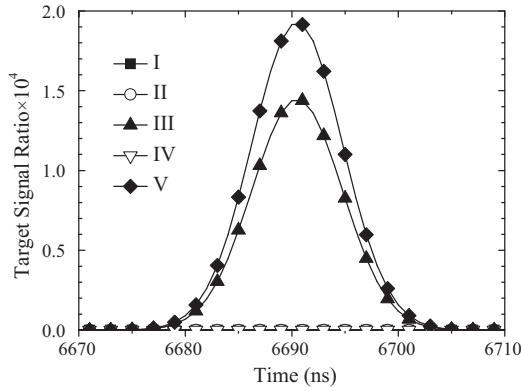


Fig. 11. Dependence of TSR on pulse time of five bands in aerosol atmosphere.

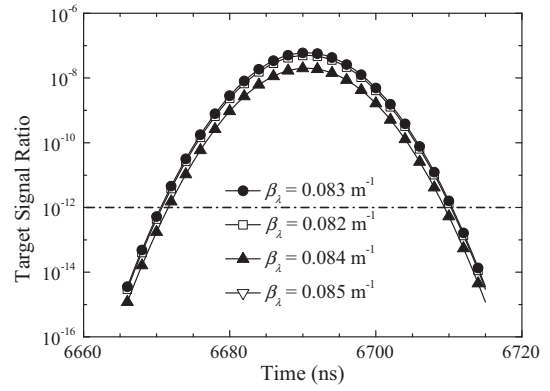


Fig. 12. Dependence of TSR on pulse time of different spectral extinction coefficients.

3.3. Radiation fog

Radiation fog is studied to discuss the effect on the double pass radiative transfer of pulse laser. The particle size distribution of radiation fog meets the Deirmenjian spectral model, which can be written as

$$n(r) = ar^\alpha \exp(-br^\beta) \tag{20}$$

where a , b , α and β are 17797.64, 8.21, 5.21 and 0.40, respectively. The average property parameters of radiation fog are calculated based on Mie scattering theory and the complex refractive index of water drop. These parameters are shown in Table 5.

Compared mean property parameters of radiation fog to urban aerosol, it can be seen that the extinction coefficient and refractive index of radiation fog are bigger than that of urban aerosol. The refractive index of radiation fog is close to 1 which means extinction effect of pulse laser is mainly manifest on the scattering. Table 6 shows the average property parameters of radiation fog at 0–1 km. It can be seen that the extinction index of band III is the smallest.

Average property parameters of radiation fog in Table 5 are used to calculate the value of ESR. The results show that the TSR of all bands are zero, i.e., the detector cannot receive the reflection energy of target surface in uniform radiation fog atmosphere condition at 0–1 km. The results of radiation fog are same to that of urban aerosol.

The optical thickness is calculated when basic calculation parameters keep constant at 0–1 km. TSR at different extinction index with a refractive index of 1.0, a mirror-diffuse ratio of 1.0 and a detective threshold of 1.0×10^{-12} is shown in Fig. 12. The whole surface of detector can receive 1.0×10^{-12} W energy when the pulse power of laser emitter is 1 W.

Table 5
Spectral mean property parameters of radiation fog.

Bands	I	II	III	IV	V
Extinction coefficient (m^{-1})	0.0134	0.026	0.0137	0.321	0.0246
Scattering coefficient	1.000	0.999	0.999	0.992	0.949

Table 6
Spectral mean property parameters of uniform radiation fog.

Bands	I	II	III	IV	V
Extinction coefficient (m^{-1})	0.134	0.0263	0.0132	0.322	0.0264
Scattering coefficient	0.999	0.998	0.993	0.989	0.885

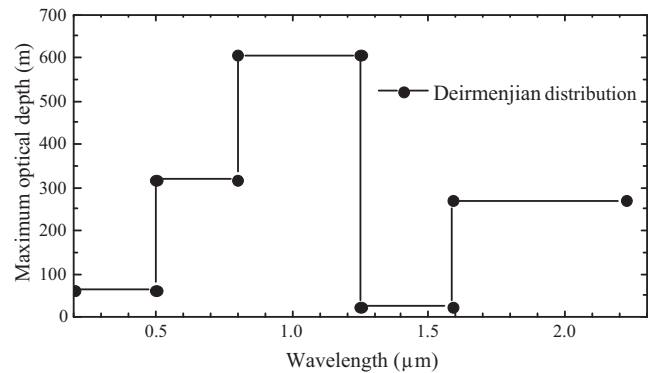


Fig. 13. Maximum detection depth as a function of wavelength.

TSR is less than the threshold when the extinction index is $0.0085 m^{-1}$. The biggest extinction coefficient is roughly set to $0.0084 m^{-1}$ at 1 km. Its maximum optical thickness of round transfer process is 16.8, confidence interval is ± 0.2 accordingly. The TSR will increase because the vertical depth of real fog is less than 1 km when it is filled with radiation fog at 0–1 km.

The maximum detector depth of each band in radiation fog is estimated, which is shown in Fig. 13. Transitive ability can be illustrated by the maximum detection depth. The optimal is band III. The following are bands II and V.

3.4. Transmission property

Transmission properties of each band at different atmosphere conditions is investigated in the above sections. Brief results of

Table 7
Transmission ability of each band at different atmosphere conditions.

Transmission ability	Standard atmosphere	Aerosol	Radiation fog
Strong	Band I	Band V	Band III
Moderate	Band II	Band III	Band II
Weak	Band III	/	Band V

transmission property are shown in Table 7. The transmission ability of band III is strongest in the typical urban aerosol and radiation fog air turbid medium, the next is band V. The optimal transmission ability occurred in bands I, V, and III on the condition of the standard atmosphere, aerosol, and radiation fog, respectively. The strong target echo signal in the above atmosphere conditions can be obtained when the detector wave length is in the range of 0.75–1.25 μm .

4. Conclusions

The model of transient radiative transfer of bidirectional path laser based on Monte Carlo method is developed to investigate the optimum wavelength of active detector at complex atmospheric conditions. It was used to calculate the effect of wavelength on the echo signal characteristic for typical atmosphere conditions, such as standard urban aerosol and radiation fog. The following conclusions are drawn:

- (1) The characteristics of radiative transfer in dispersion media for pulse laser are analyzed. Active detection conditions of pulse laser and the model of bidirectional path transient radiative transfer are proposed. Reflection characteristics of target surface are analyzed. The effect of radius of detector on ESR is studied. It is difficult to receive the reflection signal of detector surface in the condition of strong diffuse of ground and small radius of detector.
- (2) The optimal transmission property occurred in the bands I, V, and III on the condition of dry atmosphere condition, urban aerosol atmosphere condition, and radiation fog and complex atmosphere condition, respectively. Band V is the optimal choice when the detection environment is in the continental urban. Band III is the optimal choice in radiation fog. The results provide basic support to choice the optimal spectral band for active detection.

Acknowledgments

This work was supported by the National Natural Science Foundation of China (Grant Nos. 51436009 & 51406041), and the China Postdoctoral Science Special Foundation (Grant No. 2015T80347). We would like to thank the editors and referees for their comments, which helped us to improve this paper.

References

- [1] P.H. Du, D.X. Geng, W. Wang, M.L. Gong, Laser detection of remote targets applying chaotic pulse position modulation, *Opt. Eng.* 54 (11) (2015), 114102–114102.
- [2] H. Surmann, A. Nüchter, J. Hertzberg, An autonomous mobile robot with a 3D laser range finder for 3D exploration and digitalization of indoor environments, *Robot. Auton. Syst.* 45 (3) (2003) 181–198.
- [3] Y.F. Zhang, X.Q. Sun, Analysis of the restricting factors of laser countermeasure active detection technology, *Infrared Phys. Technol.* 77 (2016) 16–20.
- [4] R.X. Adhikari, Gravitational radiation detection with laser interferometry, *Rev. Mod. Phys.* 86 (1) (2014) 121.
- [5] K. Sitara, B.M. Mehre, Digital video tampering detection: An overview of passive techniques, *Digit. Invest.* 18 (2016) 8–22.
- [6] L. Sanchez, V. Ramos, O. Ledesma, Efficient detection of missing tags for passive RFID systems, *Int. J. Commun. Syst.* (2016).
- [7] Y. Li, D.K. Jha, A. Ray, T.A. Wettergren, Information fusion of passive sensors for detection of moving targets in dynamic environments, *IEEE T. Cybernetics* 47 (1) (2017) 93–104.
- [8] X. Wang, S. Wang, D. Bi, Distributed visual-target-surveillance system in wireless sensor networks, *IEEE T. Syst. Man Cy.* B 39 (5) (2009) 1134–1146.
- [9] D. Gu, A game theory approach to target tracking in sensor networks, *IEEE Trans. Syst., Man, Cybern. B, Cybern.* 41 (1) (2011) 2–13.
- [10] H.L. Wei, X.H. Chen, R.Z. Rao, Y.J. Wang, Y. Ping, A moderate-spectral-resolution transmittance model based on fitting the line-by-line calculation, *Opt. Express* 15 (13) (2007) 8360–8370.
- [11] W.Z. Wang, Y.M. Wang, W.J. Song, G.Q. Shi, Evaluation of infrared heat loss of dust-polluted surface atmosphere for solar energy utilization in mine area, *Int. J. Hydrogen Energy* 41 (35) (2016) 15892–15898.
- [12] Y.M. Wang, G.Q. Shi, Z.X. Guo, Heat transfer and thermodynamic processes in coal-bearing strata under the spontaneous combustion condition, *Numer. Heat Transfer A Appl.* 71 (1) (2017) 1–16.
- [13] Z.Z. He, L. Wei, M.H. Shao, X.N. Lu, Detection of micro solder balls using active thermography and probabilistic neural network, *Infrared Phys. Technol.* 81 (2017) 236–241.
- [14] S. Dudzik, Two-stage neural algorithm for defect detection and characterization uses an active thermography, *Infrared Phys. Technol.* 71 (2015) 187–197.
- [15] B.B. Lahiri, S. Bagavathiappan, L.T. Sebastian, J. Philip, T. Jayakumar, Effect of non-magnetic inclusions in magnetic specimens on defect detection sensitivity using active infrared thermography, *Infrared Phys. Technol.* 68 (2015) 52–60.
- [16] C.X. Zhang, H.H. Zhou, X. Chen, Y. Yuan, Y. Shuai, H.P. Tan, Three-dimensional imaging simulation of active laser detection based on DLOS method, *Infrared Phys. Technol.* 77 (2016) 73–81.
- [17] F. Christnacher, S. Schertzer, N. Metzger, E. Bacher, M. Laurenzis, R. Habermacher, Influence of gating and of the gate shape on the penetration capacity of range-gated active imaging in scattering environments, *Opt. Express* 23 (26) (2015) 32897–32908.
- [18] H. Zhang, H. Wei, H. Yang, et al., Active laser ranging with frequency transfer using frequency comb, *Appl. Phys. Lett.* 108 (18) (2016) 181101.
- [19] Y.J. Chen, K.M. Birnbaum, H. Hemmati, Active laser ranging over planetary distances with millimeter accuracy, *Appl. Phys. Lett.* 102 (24) (2013) 241107.
- [20] J.J. Degnan, Asynchronous laser transponders for precise interplanetary ranging and time transfer, *J. Geodyn.* 34 (3) (2002) 551–594.
- [21] J. Busck, H. Heiselberg, Gated viewing and high-accuracy three-dimensional laser radar, *Appl. Opt.* 43 (24) (2004) 4705–4710.
- [22] O. Steinvall, T. Carlsson, Three-dimensional laser radar modeling, *P. Sco. Photo-Opt. Ins.*, SPIE 4377 (2001) 23–34.
- [23] O. Steinvall, P. Andersson, M. Elmquist, Image quality for range-gated systems during different ranges atmospheric conditions, *Proc. SPIE* 6396 (2006) 639607.
- [24] E. Repasi, P. Lutzmann, O. Steinvall, M. Elmqvist, B. Göhler, G. Anstett, Advanced short-wave length infrared range-gated imaging for ground applications in monostatic and bistatic configurations, *Appl. Opt.* 48 (31) (2009) 5956–5969.
- [25] C.H. Wang, Y. Zhang, H.L. Yi, H.P. Tan, Transient radiative transfer in two-dimensional graded index medium by Monte Carlo method combined with the time shift and superposition principle, *Numer. Heat Tr. A-Appl.* 69 (6) (2016) 574–588.
- [26] M. Roger, C. Caliot, N. Crouseilles, et al., A hybrid transport-diffusion model for radiative transfer in absorbing and scattering media, *J. Comput. Phys.* 275 (2014) 346–362.
- [27] Z.X. Guo, S. Kumar, K.C. San, Multidimensional Monte Carlo simulation of short-pulse laser transport in scattering media, *J. Thermophys. Heat Tr.* 14 (4) (2000) 504–511.
- [28] Z.X. Guo, S. Kumar, Discrete-ordinates solution of short-pulsed laser transport in two-dimensional turbid media, *Appl. Opt.* 40 (2001) 3156–3163.
- [29] Z.X. Guo, S. Kumar, Three-dimensional discrete ordinates method in transient radiative transfer, *J. Thermophys. Heat Tr.* 16 (2002) 289–296.
- [30] J.M. Wang, C.Y. Wu, Transient radiative transfer in a scattering slab with variable refractive index and diffuse substrate, *Int. J. Heat Mass Tran.* 53 (2010) 3799–3806.
- [31] J.C. Chai, One-dimensional transient radiation heat transfer modeling using a finite-volume method, *Numer. Heat Tr. B-Fund.* 44 (2003) 187–208.
- [32] Y.H. Yun, H.D. Li, L.R.E. Wood, et al., An efficient method of wavelength interval selection based on random frog for multivariate spectral calibration, *Spectrochim. Acta A* 111 (2013) 31–36.
- [33] L.L. Bonilla, A. Glavan, A. Marquina, Wavelength selection of rippling patterns in myxobacteria, *Phys. Rev. E* 93 (1) (2016) 012412.
- [34] M. Byrd, A. Pung, E. Johnson, et al., Wavelength selection and polarization multiplexing of blue laser diodes, *IEEE Photon. Tech. L.* 27 (20) (2015) 2166–2169.
- [35] A. Tarasov, H. Chu, Solid-state laser wavelength selection and tuning by fused-silica-transmission gratings with subwavelength deep-surface relief, *Opt. Lett.* 40 (15) (2015) 3572–3575.
- [36] L.H. Liu, P. Hsu, Analysis of transient radiative transfer in semitransparent graded index medium, *J. Quant. Spectrosc. Ra.* 105 (3) (2007) 357–376.
- [37] T. Binzoni, T.S. Leung, A.H. Gandjbakche, D. Rufenacht, D.T. Delpy, The use of the Henyey-Greenstein phase function in Monte Carlo simulations in biomedical optics, *Phys. Med. Biol.* 51 (17) (2006) N313.

- [38] T.H. Roos, T.M. Harms, A new radiative transfer scattering phase function discretisation approach with inherent energy conservation, *Int. J. Heat Mass Tran.* 73 (2014) 789–803.
- [39] Y. Yuan, C.X. Zhang, L.X. Li, S.K. Dong, H.P. Tan, Multiple scattering analytical method for apparent characteristics in multilayer media, *Int. J. Heat Mass Tran.* 111 (2017) 551–558.
- [40] C.X. Zhang, Y. Yuan, T.J. Li, S.K. Dong, H.P. Tan, Analytical method to study multiple scattering characteristics in participating media, *Int. J. Heat Mass Tran.* 101 (2016) 1053–1062.
- [41] Y. Yuan, H.L. Yi, Y. Shuai, B. Liu, H.P. Tan, Inverse problem for aerosol particle size distribution using SPSO associated with multi-lognormal distribution model, *Atmos. Environ.* 45 (28) (2011) 4892–4897.
- [42] Q.J. Mao, Recent developments in geometrical configurations of thermal energy storage for concentrating solar power plant, *Renew. Sust. Energy Rev.* 59 (2015) 320–327.
- [43] L.Y. Wei, H. Qi, Y.T. Ren, L.M. Ruan, Application of stochastic particle swarm optimization algorithm to determine the graded refractive index distribution in participating media, *Infrared Phys. Technol.* 79 (2016) 74–84.